Electrochromic Supercapacitors Hot Paper

DOI: 10.1002/anie.201407365

Large-Scale Fabrication of Pseudocapacitive Glass Windows that Combine Electrochromism and Energy Storage**

*Peihua Yang, Peng Sun, Zhisheng Chai, Langhuan Huang, Xiang Cai, Shaozao Tan, Jinhui Song, and Wenjie Mai**

Abstract: *Multifunctional glass windows that combine energy storage and electrochromism have been obtained by facile thermal evaporation and electrodeposition methods. For example, WO_3 films that had been deposited on fluorine-doped tin oxide (FTO) glass exhibited a high specific capacitance of 639.8 Fg^{-1}. Their color changed from transparent to deep blue with an abrupt decrease in optical transmittance from 91.3% to 15.1% at a wavelength of 633 nm when a voltage of −0.6 V (vs. Ag/AgCl) was applied, demonstrating its excellent energy-storage and electrochromism properties. As a second example, a polyaniline-based pseudocapacitive glass was also developed, and its color can change from green to blue. A large-scale pseudocapacitive WO_3-based glass window (15 × 15 cm^2) was fabricated as a prototype. Such smart pseudocapacitive glass windows show great potential in functioning as electrochromic windows and concurrently powering electronic devices, such as mobile phones or laptops.*

The recent increase in the research of pseudocapacitors, a kind of energy-storage device, is due to its very high power density, short charging time, high energy density, long cycle life, and good stability.[1,2] Pseudocapacitance is usually associated with reversible faradic reactions at the electrode surface, through which charges are stored. When a reversible faradic reaction occurs with charge transfer, some electrode materials will reversibly change color. This phenomenon is known as electrochromism.[3] Smart windows based on electrochromism have been used in buildings, automobiles, and even in the Boeing 787 Dreamliner. As transitional-metal-oxide-based pseudocapacitors and smart electrochromic windows both make use of the reversible electrochemical reactions occurring at the electrodes, they can be integrated into a single device by deliberately choosing suitable electrochemically active materials.

Tungsten oxide (WO_3) has shown superior electrochemical performance and has been extensively investigated in the individual fields of pseudocapacitors and electrochromic devices. For instance, Jo et al. reported mesoporous WO_3/carbon materials for effective pseudocapacitors,[4] Cong et al. demonstrated fast electrochromic applications of WO_3 quantum dots,[5] and Liang et al. reported ultrathin WO_3 nanosheets for flexible electrochromic devices.[6] A few research groups have started to realize the potential of combining pseudocapacitive and electrochromic effects.[7–9] However, previous reports mainly focused on pure electrodes; an integrated stand-alone device both severing as a pseudocapacitor and a smart window has not been reported to date. Herein, the facile and scalable fabrication of supercapacitive glass windows that combine electrochromism and energy storage is demonstrated. As illustrated in Scheme 1 a, uniform ultrathin WO_3 films with high-performance pseudocapacitive behavior and fast-response electrochromism were obtained by evaporating WO_3 powder on fluorine-doped tin oxide (FTO). Afterwards, pseudocapacitive glass windows were assembled in a symmetric configuration by using the ultrathin WO_3 films as the electrodes and H_2SO_4 as the electrolyte. The large-scale pseudocapacitive glass windows present great

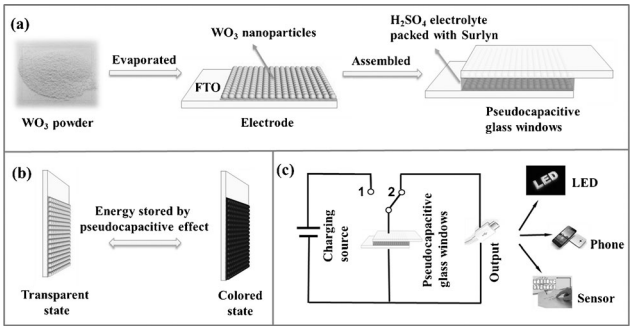

Scheme 1. a) Preparation of the WO_3 polycrystalline film and the symmetric device. b) Electrochromism of the WO_3 electrode in acid electrolyte. c) Working principle of the pseudocapacitive glass windows.

[*] P. Yang, P. Sun, Z. Chai, Prof. W. Mai
Department of Physics and Siyuan Laboratory
Jinan University
Guangzhou 510632 (China)
E-mail: wenjiemai@gmail.com
Prof. L. Huang, Dr. X. Cai, Prof. S. Tan
Department of Chemistry, Jinan University
Guangzhou 510632 (China)
Prof. J. Song
Department of Metallurgical and Materials Engineering
University of Alabama
Tuscaloosa, AL 35487 (USA)

[**] We thank Prof. Zhong Lin Wang from the Georgia Institute of Technology, Prof. Shuqin Song and Kun Wang from Sun Yat-sen University, and Prof. Weiguang Xie and Zhimin Liang from Jinan University for helpful discussions and assistance with the experiments. W.J.M. thanks the National Natural Science Foundation of China (51102115 and 21376104), the Natural Science Foundation of Guangdong Province, China (S2013010012876), and the State Key Laboratory of Optoelectronic Materials and Technologies (Sun Yat-sen University) Open Fund.

Supporting information for this article is available on the WWW under http://dx.doi.org/10.1002/anie.201407365.

potential applications in smart electrochromic windows for powering portable electronic devices, such as laptops and cell phones.

The ultrathin WO_3 film was obtained through an evaporation procedure utilizing WO_3 nanoparticle powder. A typical scanning electron microscopy (SEM) image of the product is given in Figure 1 a, showing the morphology of the

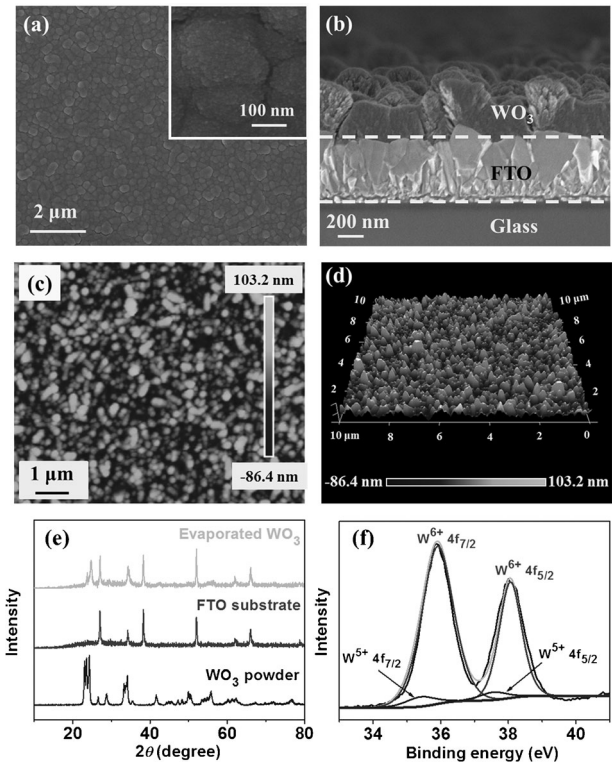

Figure 1. a) SEM image of an as-prepared WO_3 film (inset: corresponding magnified image). b) Cross-section SEM image of the WO_3 thin film evaporated on an FTO substrate. c) 2D and d) 3D AFM images of a $10\times10\ \mu m^2$ area of the WO_3 thin film. e) XRD pattern of the WO_3 thin film, suggesting the polycrystalline structure of the WO_3 thin film. The patterns of the FTO substrate and the WO_3 powder source are shown for comparison. f) XPS survey of the W 4f spectra of the WO_3 film.

WO_3 film deposited on FTO. The WO_3 grains are 100–300 nm in diameter, several times larger than the evaporation source (50 nm). A large amount of granular voids exist in these kinds of films, which is beneficial for cation storage and release. The thickness of the thin film is approximately 300 nm, which was confirmed by the cross-section SEM image as shown in Figure 1 b. Atomic force microscopy (AFM) measurements were performed to further evaluate the morphology of the WO_3 thin film. (Figure 1 c and d). The average diameter of the grains is nearly 200 nm, showing a well-distributed 3D morphology.

The X-ray diffraction (XRD) patterns (Figure 1 e) indicate that the WO_3 film has typical polycrystalline features, which allow for sufficient grain boundaries and granular voids for electrolyte penetration. The chemical composition of the as-prepared tungsten oxide on FTO was analyzed using X-ray photoelectron spectroscopy (XPS; Figure 1 f). The W 4f spectrum can be resolved into four peaks. The strong peaks located at 35.90 and 38.05 eV correspond to the W^{6+} oxidation state, whereas the weak peaks located at 35.50 and 37.60 eV correspond to the W^{5+} oxidation state.[10,11] As the intensity of the W^{6+} oxidation state is obviously stronger than that of the W^{5+} state, it can be inferred that the evaporated film consisted predominantly of WO_3.

The electrochemical study of the WO_3 film was conducted with a three-electrode configuration. A piece of film electrode (effective area 1 cm^2) was dipped into H_2SO_4 solution (1 M) at room temperature for a single electrode test. A Ag/AgCl reference electrode and a Pt counter electrode were used in the measurement. Figure 2 a shows the cyclic voltam-

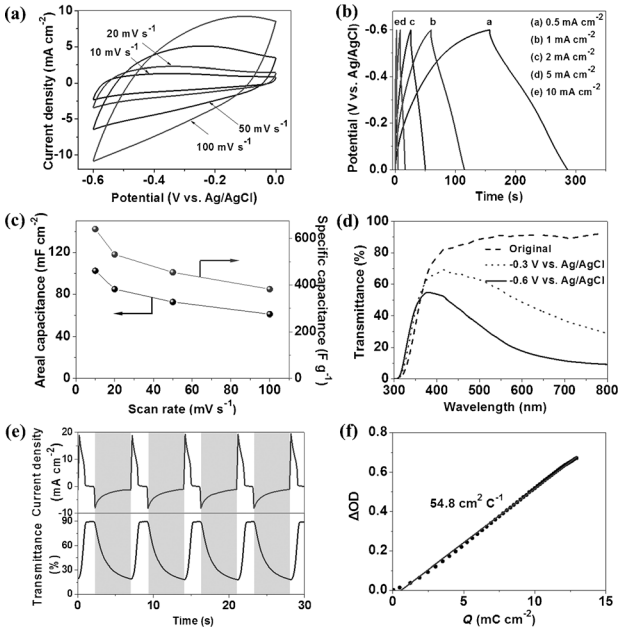

Figure 2. a) CV curves of the WO_3 film at different scan rates. b) Galvanostatic charge/discharge curves of the WO_3 electrode collected at different current densities. c) Areal and specific capacitances of the WO_3 film as functions of the scan rate. d) Transmittance spectra of deposited WO_3 electrodes for different voltage conditions. e) Chronoamperometry curve and the corresponding in situ transmittance curve at 633 nm for the WO_3 film electrode. f) Optical density versus charge density of the WO_3 electrode, which gives a coloration efficiency of 54.8 cm^2C^{-1}.

metry (CV) curves of the WO_3 electrode under different scan rates. Typical galvanostatic charge/discharge curves of the WO_3 electrode collected under different current densities are shown in Figure 2 b. It reveals that the charge curves and the corresponding discharge counterparts are symmetric, indicating good capacitive behavior of the evaporated film. Based on the CV curves, the areal and the specific capacitances were calculated (Figure 2 c). At a scan rate of 10 $mV s^{-1}$, the areal capacitance of the WO_3 electrode reached 102.4 $mF cm^{-2}$. The corresponding specific capacitance was 639.8 $F g^{-1}$, which is evidently much higher than those previously reported for tungsten oxides, such as 290 $F g^{-1}$ (25 $mV s^{-1}$) for crystalline

WO_3[12] and 199 $F g^{-1}$ (1 $mA cm^{-2}$, approximately 1 $mV s^{-1}$) for mesoporous WO_{3-x}.[13]

During the ongoing CV or galvanostatic charge/discharge electrochemical process, electrochromism was observed for the WO_3 electrode. Both the pseudocapacitive behavior and the electrochromic response are due to the redox reactions between W^{6+} and W^{5+}, which are accompanied by H^+ insertion/extraction ($WO_3 + e^- + H^+ \Leftrightarrow HWO_3$;[14] Scheme 1 b). The electrochromic optical modulation range of the WO_3 film was examined, and the obtained UV/Vis transmission spectra for its original and colored states at different potentials are shown in Figure 2 d. The electrode was transparent with an optical transmittance of 91.3 % at a wavelength of 633 nm in its the original state. However, its color changed to deep blue with a decrease in the optical transmittance to 15.1 % at the same wavelength (633 nm) when a voltage of −0.6 V (vs. Ag/AgCl electrode) was applied.

The coloration switching response is a key parameter for electrochromic materials. Chronoamperometry was performed on the WO_3 film under an alternating potential of ± 0.6 V (vs. Ag/AgCl), and the corresponding in situ transmittance is shown in Figure 2 e. The coloration and bleaching times were defined as the time required for a 90 % change in the full transmittance modulation at 633 nm.[15] For the as-prepared WO_3 film, the coloration time t_c was found to be 3.1 s, and the bleaching time t_b was 0.9 s (magnified image in the Supporting Information, Figure S1). The fast switching speed of the WO_3 particle film is possibly due to the large amount of granular voids in the film and good contact between the film and the substrate. The coloration and bleaching times are significantly shorter than those of previously reported WO_3 materials, such as hexagonal-structured WO_3 (7.6, 4.2 s)[15] and silver-decorated WO_3 thin films (3.9, 3.2 s).[16] The bleaching time is much shorter than the coloration time (shown by the asymmetric shape of the curves in Figure 2 e), disclosing that the conductivity of the WO_3 film changes during the electrochromic process. Generally, tungsten oxide is more conductive in its reduced state (colored state) than in its oxidized state (bleached state), which can be inferred from the high current density that is observed when the electrode starts to bleach.

Coloration efficiency (CE) is another crucial parameter for electrochromic materials, which is defined as the change in optical density (OD) per unit of inserted charge. The relation of the OD to the charge density is shown in Figure 2 f, and the CE can be calculated from the slope of the quasi-linear curve. A mediate CE of 54.8 $cm^2 C^{-1}$ was obtained for the WO_3 particle film, which is confined by the high-level charge storage ability during the electrochromic process. Even so, the value is comparable to those of previously reported WO_3 materials, such as amorphous (55 $cm^2 C^{-1}$)[17] and crystalline (42 $cm^2 C^{-1}$) WO_3.[18]

A symmetric pseudocapacitor device was fabricated using two WO_3 film electrodes and H_2SO_4 electrolyte (Scheme 1 a). In the CV tests, the WO_3 device showed capacitive behavior at a voltage range of 0 to 0.9 V (Figure 3 a), whereas the FTO device exhibited negligible electrochemical performance. The electrochemical behavior of the WO_3 device with H_2SO_4 electrolyte is similar to that of the WO_3 device with an

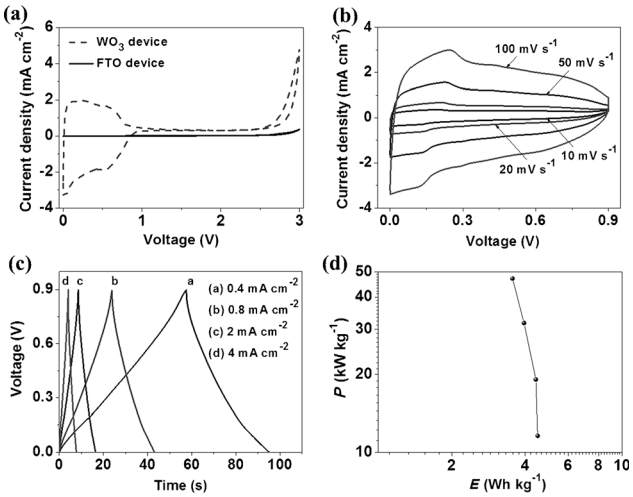

Figure 3. a) CV curves of the assembled WO_3-based pseudocapacitive glass windows and the pure FTO device collected at 100 $mV s^{-1}$ in a voltage range of 0 to 3 V. b) CV curves of the assembled WO_3 pseudocapacitor device collected at different scan rates. c) Galvanostatic charge/discharge curves of the WO_3 pseudocapacitor device collected at different current densities. d) Ragone plot of the WO_3 pseudocapacitor device.

electrolyte consisting of $LiClO_4$ and propylene carbonate (Figure S2). Figure 3 b shows the CV curves of the device that were collected at various scan rates between 10 and 100 $mV s^{-1}$ in the capacitive-behavior window. Obviously, all CV curves exhibit capacitive behavior. Galvanostatic charge/discharge curves of the device were collected under different current densities (Figure 3 c); a linearly time-dependent change in voltage at a constant current can been seen, which is a characteristic of pseudocapacitors or so-called oxide supercapacitors.[2] Power density and energy density are two important parameters of a pseudocapacitor device. The energy densities were calculated using the method of integrating discharge curves.[19] Figure 3 d shows the Ragone plot of the WO_3 symmetric device. The active material of the device exhibited a high power density of 47.1 $kW kg^{-1}$, which is much higher than those recently reported for 3D graphene hydrogel symmetric supercapacitors (0.7 $kW kg^{-1}$),[20] MnO_2–ERGO//CNT–ERGO asymmetric supercapacitors (0.9 $kW kg^{-1}$),[21] 3D graphene//Fe_3O_4–graphene asymmetric supercapacitors (2.6 $kW kg^{-1}$),[22] and MnO_2–graphene//graphene asymmetric supercapacitors (5 $kW kg^{-1}$).[23] A corresponding energy density of 3.6 $Wh kg^{-1}$ was obtained, which was limited by the cell voltage. If an asymmetric configuration is implemented by prudently choosing the positive electrode, high energy densities will be achieved.[24–26] Five devices connected in series can light a red LED (Figure S3 a, insets), indicating broad applications in microelectronics and daily life.

Areal and specific capacitances were calculated (Figure S3 a). At a current density of 0.4 $mA cm^{-2}$, the areal capacitance of the device reached 12.8 $mF cm^{-2}$. The corresponding specific capacitance was 160.1 $F g^{-1}$ for the WO_3 material in a device configuration. Moreover, it is noteworthy that the device retains 78.9 % of its initial capacitance when

the current density was increased from 0.4 to 4 mA cm^{-2}, showing excellent rate capability. Furthermore, the device also showed good cycle stability. According to Figure S3b, more than 95% of the initial capacitance were retained after 5000 cycles, which is a decisive factor in practical applications.

In the device configuration, electrochromic behavior occurred at about 2.5 V (Figure 3a and S2). From the transmittance spectra given in Figure 4a, it can be seen that the optical transmittance of the WO_3 pseudocapacitive glass windows is 78.8% in the original state and 15.1% in the colored state (3 V) at a wavelength of 633 nm. The device has an optical transmittance change of 63.7%. In Figure 4b, indoor and outdoor demonstrations of the electrochromic behavior of a large-scale pseudocapacitive glass window (15 × 15 cm^2) are displayed. Glass with electrochromic behavior is an energy-saving building material and can efficiently solve the light pollution problem. Its color changes along with the voltage applied, and the glass can thus be used to modulate the incoming natural light to preserve privacy without using blinds and curtains. Our newly-designed pseudocapacitive glass windows not only retain the above-mentioned electrochromism, but also feature further impressive properties, such as energy storage. Pseudocapacitive glass windows that can power electronic devices, such as LEDs, mobile phones, iPads, and sensors, and control the transmittance at the same time might make our lives more convenient (Scheme 1c). By further combining the pseudocapacitive glass windows with solar cells, nanogenerators, and other energy supplies, self-powered systems can be implemented, which can improve the efficiency of energy conversion and storage.[27–30]

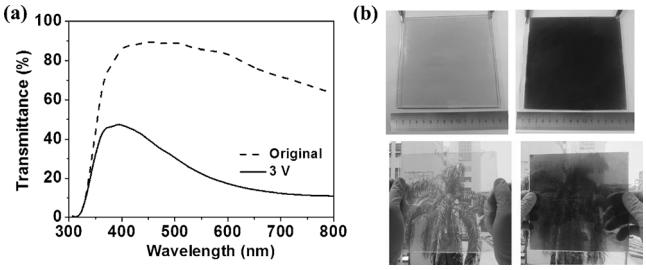

Figure 4. a) Transmittance spectra of the WO_3-based pseudocapacitive glass windows under original and charged conditions. b) Indoor and outdoor demonstrations of large-scale WO_3-based pseudocapacitive glass windows.

It should be noted that WO_3 is not the only material that can be used for both pseudocapacitor and electrochromic devices. To demonstrate the universality of this kind of integration design, polyaniline (PANI) nanowire networks were also fabricated through electrodeposition (Figure S4).[31] The PANI nanowire networks can be uniformly deposited on an FTO substrate, with an average diameter of approximately 100 nm. A device was assembled using two PANI electrodes and H_2SO_4 electrolyte and featured a light green color. When the symmetric device was charged to 0.8 V, the color changed to a light blue, indicating good electrochromic behavior. Furthermore, the assembled PANI device demonstrated good capacitive behavior. This is another example of pseudocapacitive glass windows with integrated electrochromic functionality.

In summary, a multifunctional large-scale glass window that integrates energy storage and electrochromism was designed by depositing WO_3 films or PANI nanowire networks by thermal evaporation or electrodeposition. Specifically, WO_3 films deposited on FTO glass exhibited a high specific capacitance of 639.8 F g^{-1}, and their optical transmittance abruptly decreased from 91.3% to 15.1% at a wavelength of 633 nm when a voltage of −0.6 V was applied. A large-scale pseudocapacitive WO_3-based glass window (15 × 15 cm^2) was also prepared. Such pseudocapacitive glass windows show great potential in functioning as electrochromic smart windows and concurrently powering electronic devices, such as LEDs, mobile phones, iPads, and sensors, which should have a profound impact on our daily life in the future.

Received: July 18, 2014
Published online: September 11, 2014

Keywords: electrochromism · energy storage · metal oxides · pseudocapacitors · supercapacitors

[1] V. Augustyn, P. Simon, B. Dunn, *Energy Environ. Sci.* **2014**, *7*, 1597.
[2] P. Simon, Y. Gogotsi, B. Dunn, *Science* **2014**, *343*, 1210.
[3] C. G. Granqvist, *Thin Solid Films* **2014**, *564*, 1.
[4] C. Jo, J. Hwang, H. Song, A. H. Dao, Y.-T. Kim, S. H. Lee, S. W. Hong, S. Yoon, J. Lee, *Adv. Funct. Mater.* **2013**, *23*, 3747.
[5] S. Cong, Y. Tian, Q. Li, Z. Zhao, F. Geng, *Adv. Mater.* **2014**, *26*, 4260.
[6] L. Liang, J. Zhang, Y. Zhou, J. Xie, X. Zhang, M. Guan, B. Pan, Y. Xie, *Sci. Rep.* **2013**, *3*, 1936.
[7] Z. Wei, K. Wang, H. Wu, Y. Meng, Y. Zhang, *Energy Environ. Sci.* **2012**, *5*, 8384.
[8] Z. Xie, X. Jin, G. Chen, J. Xu, D. Chen, G. Shen, *Chem. Commun.* **2014**, *50*, 608.
[9] X. Xia, D. Chao, X. Qi, Q. Xiong, Y. Zhang, J. Tu, H. Zhang, H. J. Fan, *Nano Lett.* **2013**, *13*, 4562.
[10] X. Lu, T. Zhai, X. Zhang, Y. Shen, L. Yuan, B. Hu, L. Gong, J. Chen, Y. Gao, J. Zhou, Y. Tong, Z. L. Wang, *Adv. Mater.* **2012**, *24*, 938.
[11] P. Yang, Y. Li, Z. Lin, Y. Ding, S. Yue, C. P. Wong, X. Cai, S. Tan, W. Mai, *J. Mater. Chem. A* **2014**, *2*, 595.
[12] K.-H. Chang, C.-C. Hu, C.-M. Huang, Y.-L. Liu, C.-I. Chang, *J. Power Sources* **2011**, *196*, 2387.
[13] S. Yoon, E. Kang, J. K. Kim, C. W. Lee, J. Lee, *Chem. Commun.* **2011**, *47*, 1021.
[14] G. A. Niklasson, C. G. Granqvist, *J. Mater. Chem.* **2007**, *17*, 127.
[15] J. Zhang, J.-p. Tu, X.-h. Xia, X.-l. Wang, C.-d. Gu, *J. Mater. Chem.* **2011**, *21*, 5492.
[16] R. R. Kharade, S. S. Mali, S. P. Patil, K. R. Patil, M. G. Gang, P. S. Patil, J. H. Kim, P. N. Bhosale, *Electrochim. Acta* **2013**, *102*, 358.
[17] S.-H. Lee, H. M. Cheong, C. E. Tracy, A. Mascarenhas, A. W. Czanderna, S. K. Deb, *Appl. Phys. Lett.* **1999**, *75*, 1541.
[18] S. H. Lee, R. Deshpande, P. A. Parilla, K. M. Jones, B. To, A. H. Mahan, A. C. Dillon, *Adv. Mater.* **2006**, *18*, 763.
[19] P. Yang, W. Mai, *Nano Energy* **2014**, *8*, 274.
[20] Y. Xu, Z. Lin, X. Huang, Y. Liu, Y. Huang, X. Duan, *ACS Nano* **2013**, *7*, 4042.

[21] Z. Zhang, F. Xiao, L. Qian, J. Xiao, S. Wang, Y. Liu, *Adv. Energy Mater.* **2014**, DOI: 10.1002/aenm.201400064.
[22] F. Zhang, T. Zhang, X. Yang, L. Zhang, K. Leng, Y. Huang, Y. Chen, *Energy Environ. Sci.* **2013**, *6*, 1623.
[23] Z.-S. Wu, W. Ren, D.-W. Wang, F. Li, B. Liu, H.-M. Cheng, *ACS Nano* **2010**, *4*, 5835.
[24] J. W. Long, D. Bélanger, T. Brousse, W. Sugimoto, M. B. Sassin, O. Crosnier, *MRS Bull.* **2011**, *36*, 513.
[25] X. Xiao, T. Ding, L. Yuan, Y. Shen, Q. Zhong, X. Zhang, Y. Cao, B. Hu, T. Zhai, L. Gong, J. Chen, Y. Tong, J. Zhou, Z. L. Wang, *Adv. Energy Mater.* **2012**, *2*, 1328.
[26] P. Yang, Y. Ding, Z. Lin, Z. Chen, Y. Li, P. Qiang, M. Ebrahimi, W. Mai, C. P. Wong, Z. L. Wang, *Nano Lett.* **2014**, *14*, 731.
[27] X. Xiao, T. Li, P. Yang, Y. Gao, H. Jin, W. Ni, W. Zhan, X. Zhang, Y. Cao, J. Zhong, L. Gong, W.-C. Yen, W. Mai, J. Chen, K. Huo, Y.-L. Chueh, Z. L. Wang, J. Zhou, *ACS Nano* **2012**, *6*, 9200.
[28] P. Yang, X. Xiao, Y. Li, Y. Ding, P. Qiang, X. Tan, W. Mai, Z. Lin, W. Wu, T. Li, H. Jin, P. Liu, J. Zhou, C. P. Wong, Z. L. Wang, *ACS Nano* **2013**, *7*, 2617.
[29] L. Yuan, X. Xiao, T. Ding, J. Zhong, X. Zhang, Y. Shen, B. Hu, Y. Huang, J. Zhou, Z. L. Wang, *Angew. Chem. Int. Ed.* **2012**, *51*, 4934; *Angew. Chem.* **2012**, *124*, 5018.
[30] Z. Yu, J. Thomas, *Adv. Mater.* **2014**, *26*, 4279.
[31] Z. Niu, P. Luan, Q. Shao, H. Dong, J. Li, J. Chen, D. Zhao, L. Cai, W. Zhou, X. Chen, S. Xie, *Energy Environ. Sci.* **2012**, *5*, 8726.

